# Split-Ring Resonator-Based Sensors on Flexible Substrates for Glaucoma Monitoring

**Gizem Ekinci[a], Aybuke Calikoglu[a], Sinem Nimet Solak[a], Arda Deniz Yalcinkaya[a,b], Gunhan Dundar[a], Hamdi Torun[a,b]**

[a]*Department of Electrical and Electronics Engineering, Bogazici University, Bebek 34342 Istanbul, Turkey*
[b]*Center for Life Sciences and Technologies, Bogazici University, Kandilli 34684 Istanbul, Turkey*

Corresponding author: hamdi.torun@boun.edu.tr, +90-212-359-6895

**Abstract.** Glaucoma is an eye disease that may cause blindness by damaging the optic nerve due to elevation of the intraocular pressure. Patients with glaucoma require monitoring of intraocular pressure. This paper presents split-ring resonator-based strain sensors designed and characterized for glaucoma detection application. The geometry of the sensor is optimized such that it can be embedded in a conventional contact lens. Silver conductive paint is used to form the sensors realized on flexible substrates made of cellulose acetate and latex rubber. The devices are excited and interrogated using a pair of monopole antennas. Scattering parameters are measured between the ports of the antennas, and the characteristics of devices with different curvature profiles are obtained. Finite-element based models are developed to analyse the operation of the devices and to optimize the sensor structure. The sensitivity of the device, i.e. the change in resonant frequency for a unit change in radius of curvature, on acetate film is experimentally characterized as -4.73 MHz/mm and the sensitivity of the device on latex is 33.2 MHz/mm. The experimental results supported by finite-element based models indicate that the demonstrated device is suitable for glaucoma diagnosis and monitoring.

**Keywords.** (split-ring resonator; metamaterial; biosensor; glaucoma; microwave sensor)

## 1. Introduction

Metamaterials exhibit electromagnetic properties, which are not present in ordinary materials, such as negative values of electric permittivity and magnetic permeability, simultaneously [1]. The unique properties bring metamaterials into consideration for sensing applications. One of the most popular

structures of metamaterials is split-ring resonators (SRRs). A conventional SRR is simply a ring with a split, which is made of a preferably high-conductivity metal, and is fabricated on a dielectric substrate. In addition to their favorable electromagnetic characteristics, the SRR devices can be realized in a simple and cost-effective manner.

Wireless strain measurement attracts attention of many researchers and finds application in numerous fields when it comes to material characterization. In civil engineering, the sensors of the sort are used to ensure maintenance in infrastructure, by measuring the strain on the structure and take precaution in case of any abnormal strain [2]. In biomedical engineering, these sensors are utilized by observation of the healing process of a fractured bone [3]. Moreover, in aerospace industry, wireless strain measurement comes into prominence in crack or abnormal strain detection on metal surfaces [4]. SRR-based sensors have been demonstrated for wireless strain measurement previously [3–6]. The resonant frequency of the device strongly depends on the geometry of the ring and any deviation in geometry due to external strain applied to the device results in change in resonant frequency of the resonator. This enables strain measurement through the observation of the shift in resonant frequency.

Glaucoma is an eye disease, which may damage the optic nerves and leads to vision loss. Even though it might be caused by different factors, in most of the patients, it is caused by the increase of intraocular pressure and might eventually cause irreversible blindness. Today, there are several different methods to detect the symptoms of glaucoma, such as measuring central corneal thickness [7], measuring peripheral vision [8], examining the optic nerve [9] and measuring the eyeball pressure [10,11]. Continuous monitoring of intraocular pressure enables assessing accurately the progress of the disease [12].Recently, noninvasive monitoring of the intraocular pressure has been demonstrated using piezoresistive [13] and capacitive [14] sensors embedded on soft contact lenses. An active strain sensor is placed at a specific location on a contact lens in this approach to detect the deformation of the eyeball due to the changes in intraocular pressure. It is possible to monitor the progress of the disease in noninvasive and continuous manner using this approach. However, these sensors are electrically active and require application of electrical signals in the contact lens during operation. In addition, the system on the contact lens also includes a transmission circuitry to send the signals to an external unit. Different contact lenses have been developed to cover the sclera or only cornea. The sclera is the white and opaque outer layer of the eye as schematically shown in Fig 1. It is continuous with the clear layer, the cornea, at the center. In one implementation, the sensor is placed at corneo-scleral junction for the measurements [15]. On the other hand, it was demonstrated that the radius of curvature of the sclera is well correlated with the intraocular pressure, while the radius of the curvature of the cornea is insensitive to the changes in intraocular pressure based on a study with porcine eyes [16].

Here, we describe an electrically passive, wireless and low cost sensor to measure intraocular pressure by placing an SRR on top of contact lenses. The sensor on the lens does not require any electrical signal to operate and are interrogated by external antennas that can be located away from the contact lens. We use silver conductive paint to define the rings on flexible substrates. We realized two different SRR-based strain sensors and characterized them experimentally to evaluate their potential

for wireless strain sensing. Also, we developed finite-element method-based models for the sensors. This study suggests that SRR-based sensors are promising for the diagnosis and continuous monitoring of glaucoma.

## 2. Materials and Methods

### *2.1. Design and Fabrication of the SRR-based Sensors*

The structure of a basic SRR comprises a metallic ring, circular or rectangular, with a narrow split. The structure behaves like an RLC circuit under the excitation of external electromagnetic waves. The resonator supports circulating current along the metallic ring when the magnetic field is perpendicular to its surface. So, a resonant behavior is observed at a specific frequency ($f_0$) that is determined by the geometry of the structure since the equivalent resistance, inductance and the capacitance of the ring are determined by its geometry. This is known as magnetic resonance of SRRs and the change in the resonant frequency can be utilized as a sensing parameter. The resonant frequency of an SRR is simply given in equation 1.

$$f_0 = \frac{1}{2\pi\sqrt{LC}} \tag{1}$$

where $L$ and $C$ are the equivalent inductance and the equivalent capacitance of the ring.

The equivalent capacitance of the ring has two components, the gap capacitance and surface capacitance. The gap capacitance is determined by the split region and the surface capacitance is associated with the surface charges of a metallic ring. The equivalent inductance and the equivalent capacitance can be calculated using analytical expressions for the calculation of the resonant frequency of an SRR [17].

We designed the geometry of the SRR structure so that it can be placed around the boundary between cornea and sclera where the change in intraocular pressure can be measured effectively to diagnose glaucoma. In addition, the sensor is optimized for S-band (2-4 GHz) of the electromagnetic band. Fig. 2(a) shows a photograph of a sensor placed on a flexible substrate with a thickness of 100 $\mu$m made of cellulose acetate. We extended the gap region to increase the gap capacitance and to keep the resonant frequency of the device in S-band. We realized SRR sensors using a very low cost method on different flexible substrates. We applied a negative hard mask on the substrate and we applied silver conductive paint manually using a fine brush to define SRR structure. The thickness of the ring is 50 $\mu$m, the inner radius of the ring resonator is 6 mm and the other relevant geometrical parameters are shown in Fig. 2(a). It is reported that the normal pupil radius is between 2 and 4 mm in the dark [18]. Therefore, the ring resonator does not affect the patient's vision. In addition, we prepared another type of sensor on a spherically deformed substrate made of latex rubber with a thickness of 50 $\mu$m. Using a hard mask on a spherical substrate is not possible, so we painted directly the ring on the second substrate manually using fine brush. The substrates that we use in this work are biocompatible. The SRR structure is made of silver nanoparticles, the biocompatibility of which has

been studied before [19]. We do not foresee a significant problem using silver nanoparticles since the contact lenses will be worn for 24 hours in a typical use case. In addition, the silver nanoparticle layer can be buried inside a laminated substrate.

### *2.2. Simulation and Experimental Characterization of the SRR-based Sensors*

We simulated the device using commercially available electromagnetic simulation software (CST Microwave Studio, Darmstadt, Germany) to obtain its scattering parameters. We performed the simulations in time domain. We developed realistic models for the operation of the sensors including the antennas. We modeled a pair of dipole antennas with the sensors for this purpose. We extracted the scattering parameters while introducing mechanical deformation to the substrate of the sensors.

We experimentally characterized the fabricated SRR-based strain sensors using a vector network analyzer (ZVB4, Rohde & Schwarz, Munich, Germany) by measuring their scattering parameters. We conducted the experiments using two different setups. The setups are suitable for introducing different deformation profiles to the structures shown in Fig. 3(a) and Fig. 3(b). We changed the spherical radius of curvature of the latex rubber substrate by pumping air in and out to mimic the IOP action on the eye and we changed the cylindrical radius of curvature of the cellulose acetate substrate to show that the resonant frequencies of the resonators change with both types of curvature profiles.

We used a pair of monopole patch antennas with a length of 30 mm and a width of 3.5 mm to excite the resonators during the experiments. The distance between two antennas is 10 cm. The device on the cellulose acetate was placed on an adjustable frame to introduce controllable bending between two monopole antennas as shown in Fig. 3(a). The substrate of the device on latex rubber was stretched on top of a cylindrical injection syringe with a diameter of 9 mm. The syringe was used to pump air in and out of the device. First, we pumped air so that the radius of the curvature of the substrate became 13 mm. Then, we painted the SRR structure on the surface and obtained its s21 spectrum using the vector network analyzer as shown in Fig. 3(b). We measured the air-inflated height and calculated the radii of the curvature of the latex rubber using spherical cap formulas. We continued the following measurements by evacuating 0.2 ml air at each step and obtaining the s21 spectrum of the device.

## 3. Results and Discussions

Fig. 2(b) shows the sensor structure and the simulated surface current density along the conductor path defined on cellulose acetate at the resonant frequency observed at 2.54 GHz. The magnetic field is perpendicular to the surface of the device for the simulation that supports the circulating current at resonance. Fig. 2(c) shows the s21 spectrum of the device with these settings. The nominal resonant frequency of the device was measured as 2.49 GHz, which is in good agreement with our simulations.

We investigated the change in s21 spectrum by introducing different radii of curvature to the substrate for the structure defined on cellulose acetate. The simulated and measured s21 spectra of the sensor with various radii of curvature are shown in Fig. 4(b) and Fig. 4(e), respectively. Through

simulations, we observed a circulating current profile at each resonant frequency indicating magnetic resonance, and the off-resonance magnitude level of s21 is determined by the characteristics of the antennas. The gap size of the device does not change significantly with curvature. However, the surface capacitance that is one of the components of the equivalent capacitance decreases as the projected area of the bent device on the plane of antennas decreases with curvature, which results in increasing resonant frequency and quality factor. Moreover, we repeated the bending experiment repeated six times and report the standard error mean using the error bars of Fig. 4(f). The resonant frequency of the device increases with curvature as we observed in our experiments and simulations. A linear variation for relatively small values of curvature is observed in both simulation and the experimental results. As the curvature becomes larger, the operation of the sensor deviates from the expected response of an SRR structure since the magnetic field vector that is perpendicular to the original plane of the substrate cannot support circulating current along the conductive path as the magnetic field vector inclines with it.

Moreover, we simulated and measured the s21 spectrum of the second sensor that was realized on a latex rubber to investigate the effect of the change in the radius of curvature on the transmission parameters. The computational domain of the structure is shown in Fig. 5(a). We kept the dipole antennas in this model as well for the excitation of the SRR and the measurement of s21 spectra. We defined the sensor on a section of a sphere, the curvature of which was varied. Moreover, we used the second setup to characterize the SRR sensor realized on the substrate of latex rubber. The SRR structure is defined on an inflatable latex rubber substrate and the structure shrinks as the radius of the curvature of the substrate decreases. This results in a decrease in gap width ($g$ of Fig. 2(a)). So, the gap capacitance increases, due to which the resonant frequency decreases. We repeated this experiment six times with different SRR structures painted on the substrate each time separately after we pumped air such that the radius of the curvature became 13 mm. The simulation and experimental results show that the resonant frequency of the sensor decreases with the decreasing radius of curvature as shown in Fig. 5(b) and 5(e) respectively. Lower values of quality factor with this device are observed as compared to the previous one. Fig. 5(f) also shows the mean values and the standard error mean values of the measured resonant frequencies normalized to the value we measured for the radius of curvature of 13 mm.

The range of the change in radius of the curvature is physiologically relevant to the diagnosis of glaucoma. The result of an experiment conducted with 16 fresh porcine eyes, by applying five consecutive incremental 100μl injections, suggests that with each incremental injection of fluid, intraocular pressure and radius of curvature of the sclera increases linearly from 9mm to 13mm [16].

## 4. Conclusion

Split-ring resonator-based strain sensors enable realization of wireless strain sensors that are electrically passive. In this study, we demonstrate the feasibility of detecting glaucoma using SRR sensors realized on flexible substrates that can be integrated into contact lenses. The sensors are

fabricated simply using silver conductive paint and it is also possible to use other low-cost fabrication methods to define the metallic ring structures on flexible substrates. The scattering parameters of the sensors are measured using external antennas. We use monopole patch antennas defined on standard FR4 substrates to interrogate the sensors wirelessly. It is advantageous to use electrically passive sensors on contact lenses that can be worn safely. In addition, the low-cost sensors are suitable in a disposable usage setting. We envision the use of these sensors for continuous monitoring of glaucoma.

We present two devices with different substrates that are suitable for distinct curvature profiles. The resonant frequencies of the devices depend on the curvature and the devices exhibit monotonic variation with respect to change in radius of curvature. We analyzed the electromagnetic characteristics of these sensors using finite-element method-based models.

The first device, depicted in Fig. 4(d), has a sensitivity of -4.73 MHz/mm. We measure the quality factor of the resonators on the order of 500. This corresponds to a frequency resolution of 5 MHz. Given the sensitivity values, the change in cylindrical radius of curvature of the first SRR sensor can be measured with a resolution of 1.1 mm. The sensitivity of the second device, illustrated in Fig. 5(d), is obtained as 33.2 MHz/mm and the measurement resolution for the spherical radius of curvature corresponds to 150 $\mu$m. The demonstrated device is promising towards a novel method for continuous monitoring of glaucoma.

**Acknowledgements**

This work was supported by the TUBITAK [grant number 112E250].

**References**

[1] D. Schurig, J.J. Mock, B.J. Justice, S. a Cummer, J.B. Pendry, a F. Starr, D.R. Smith, Metamaterial electromagnetic cloak at microwave frequencies., Science (80-. ). 314 (2006) 977–980. doi:10.1126/science.1133628.

[2] G. Nagayama, Tomomori;Ruiz-Sandoval, Manuel; Spencer, Bill F.;Mechitov, Kirill A.; Agha, Wireless strain sensor development for civil infrastructure, in: Trans. Soc. Instrum. Control Eng., 2004.

[3] R. Melik, N.K. Perkgoz, E. Unal, C. Puttlitz, H.V. Demir, Bio-implantable passive on-chip RF-MEMS strain sensing resonators for orthopaedic applications, J. Micromechanics Microengineering. 18 (2008) 115017. doi:10.1088/0960-1317/18/11/115017.

[4] A. Kaur, A. Marwaha, Crack Detection on Metal Surfaces with an Array of Complementary Split Ring Resonators, 119 (2015) 16–19.

[5] A.M. Albishi, M.S. Boybay, O.M. Ramahi, Complementary split-ring resonator for crack detection in metallic surfaces, IEEE Microw. Wirel. Components Lett. 22 (2012) 330–332. doi:10.1109/LMWC.2012.2197384.

[6] J. Li, W. Withayachumnankul, S. Chang, D. Abbott, Metamaterial-based strain sensors, Proc. 2011 7th Int. Conf. Intell. Sensors, Sens. Networks Inf. Process. ISSNIP 2011. (2011) 30–32. doi:10.1109/ISSNIP.2011.6146571.

[7] N.G. Congdon, A.T. Broman, K. Bandeen-Roche, D. Grover, H.A. Quigley, Central Corneal Thickness and Corneal Hysteresis Associated With Glaucoma Damage, Am. J. Ophthalmol. 141 (2006) 868–875. doi:10.1016/j.ajo.2005.12.007.

[8] R.P. Mills, N.K. Janz, P.A. Wren, K.E. Guire, Correlation of Visual Field With Quality-Of-Life Measures at Diagnosis in The Collaborative Initial Glaucoma Treatment Study (CIGTS), J. Glaucoma. (2001). doi:10.1097/00061198-200106000-00008.

[9] M. Seong, K.R. Sung, E.H. Choi, S.Y. Kang, J.W. Cho, T.W. Um, Y.J. Kim, S.B. Park, H.E. Hong, M.S. Kook, Macular and peripapillary retinal nerve fiber layer measurements by spectral domain optical coherence tomography in normal-tension glaucoma, Investig. Ophthalmol. Vis.

Sci. 51 (2010) 1446–1452. doi:10.1167/iovs.09-4258.
[10] N.R. Kim, C.Y. Kim, H. Kim, G.J. Seong, E.S. Lee, Comparison of goldmann applanation tonometer, noncontact tonometer, and TonoPen XL for intraocular pressure measurement in different types of glaucomatous, ocular hypertensive, and normal eyes., Curr. Eye Res. 36 (2011) 295–300. doi:10.3109/02713683.2010.542865.
[11] A.F. Resende, E.S. Yung, M. Waisbourd, L.J. Katz, Monitoring intra ocular pressure in glaucoma: Current recommendations and emerging cutting-edge technologies, Expert Rev. Ophthalmol. (2015). doi:10.1586/17469899.2015.1100539.
[12] E. Hughes, P. Spry, J. Diamond, 24-Hour Monitoring of Intraocular Pressure in Glaucoma Management: a Retrospective Review., J. Glaucoma. (2003). doi:10.1097/00061198-200306000-00009.
[13] M. Leonardi, P. Leuenberger, D. Bertrand, A. Bertsch, P. Renaud, First steps toward noninvasive intraocular pressure monitoring with a sensing contact lens, Invest. Ophthalmol. Vis. Sci. 45 (2004) 3113–3117. doi:10.1167/iovs.04-0015.
[14] D. Piso, P. Veiga-Crespo, E. Vecino, Modern Monitoring Intraocular Pressure Sensing Devices Based on Application Specific Integrated Circuits, J. Biomater. Nanobiotechnol. 3 (2012) 301–309. doi:10.4236/jbnb.2012.322037.
[15] K. Mansouri, F.A. Medeiros, A. Tafreshi, R.N. Weinreb, Continuous 24-Hour Monitoring of Intraocular Pressure Patterns With a Contact Lens Sensor, Arch. Ophthalmol. (2012). doi:10.1001/archophthalmol.2012.2280.
[16] B.K. Pierscionek, M. Asejczyk-Widlicka, R. a Schachar, The effect of changing intraocular pressure on the corneal and scleral curvatures in the fresh porcine eye., Br. J. Ophthalmol. 91 (2007) 801–3. doi:10.1136/bjo.2006.110221.
[17] O. Sydoruk, E. Tatartschuk, E. Shamonina, L. Solymar, Analytical formulation for the resonant frequency of split rings, J. Appl. Phys. 105 (2009). doi:10.1063/1.3056052.
[18] R.H. Spector, The Pupils, Clin. Methods Hist. Phys. Lab. Exam. (1990) 300–304. doi:10.1016/B978-1-4557-3984-4.00205-0.
[19] M.C. Stensberg, Q. Wei, E.S. McLamore, D.M. Porterfield, A. Wei, M.S. Sepúlveda. Toxicological studies on silver nanoparticles: challenges and opportunities in assessment, monitoring and imaging, Nanomedicine 6 (2011), 879–898. doi: 10.2217/nnm.11.78

**Figure Captions**

Figure 1. The cross-sectional view of an eyeball illustrating the effect of the intraocular pressure (IOP) on the fibrous layer of the eye.

Figure 2. (a) A photograph of a realized device on a substrate made of cellulose acetate, (b) Simulated distribution of surface current density for the device at resonance, (c) Simulated s21 spectrum of the device.

Figure 3. The experimental setups for the SRR sensor realized on (a) cellulose acetate, (b) latex rubber.

Figure 4. (a) The computational domain for the SRR sensor realized on cellulose acetate, (b) Simulated s21 spectra of the device with increasing curvature, (c) Variation of the resonant frequency as a function of curvature with respect to simulation results, (d) Three-dimensional drawing of the experimental setup for the SRR sensor realized on cellulose acetate, (e) s21 spectra of the device as the curvature ($1/\rho$) increases, (f) Variation of the resonant frequency as a function of curvature.

Figure 5. (a) The computational domain for the SRR sensor realized on latex rubber, (b) Simulated s21 spectra of the device with decreasing radius of curvature, (c) Variation of the resonant frequency as a function of radius of curvature with respect to simulation results, (d) Three-dimensional drawing of the experimental setup for the SRR sensor realized on latex rubber, (e) s21 spectra of the device as the curvature ($1/\rho$) increases, (f) Variation of the resonant frequency as a function of radius of curvature.

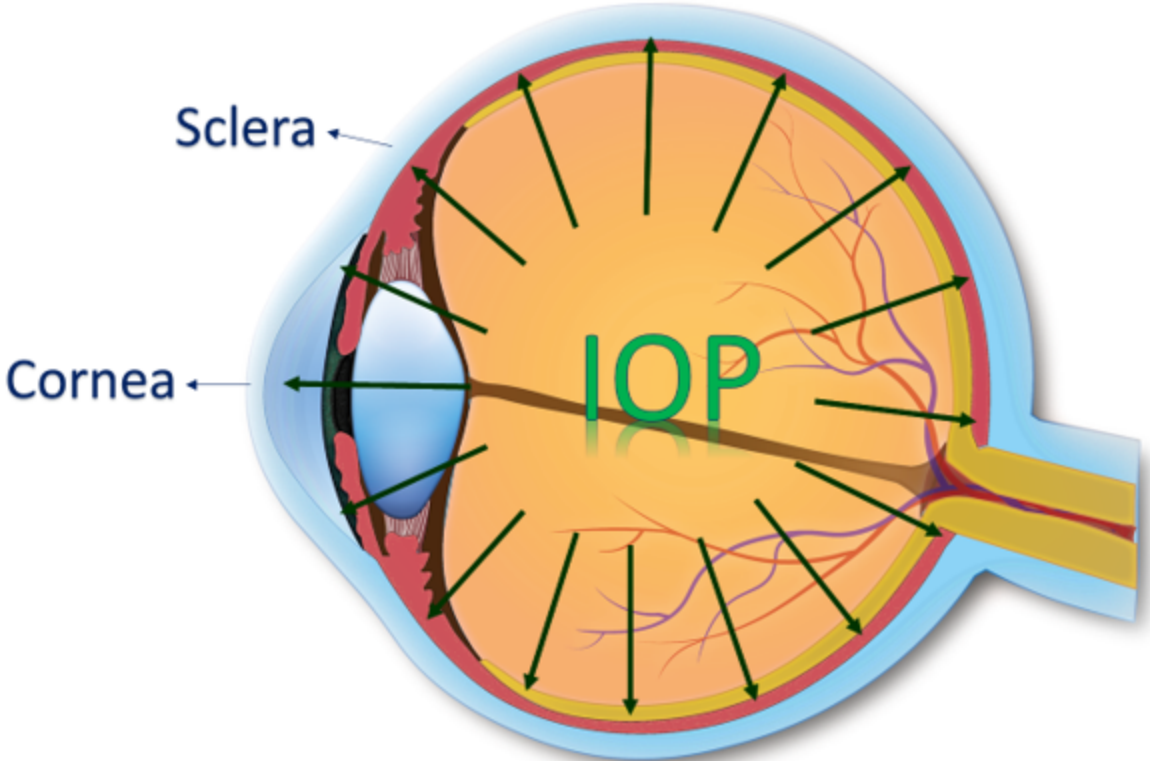
Sclera
Cornea
IOP

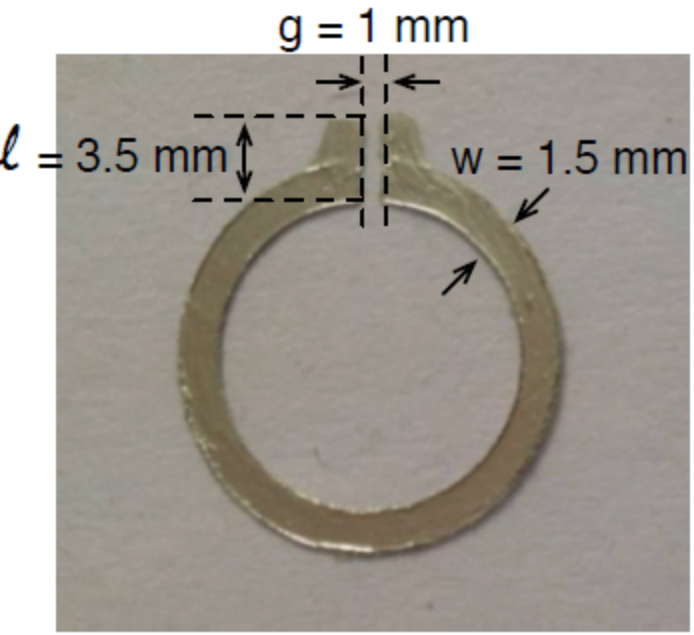
g = 1 mm
ℓ = 3.5 mm
w = 1.5 mm

(a)

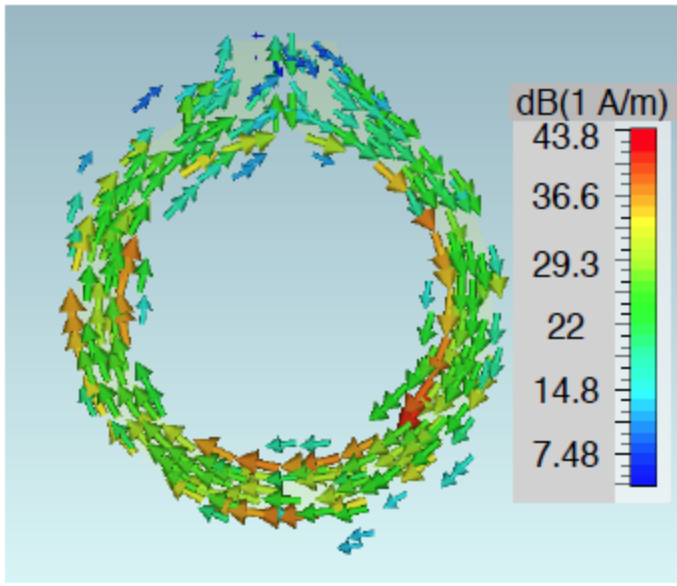
dB(1 A/m)
43.8
36.6
29.3
22
14.8
7.48

(b)

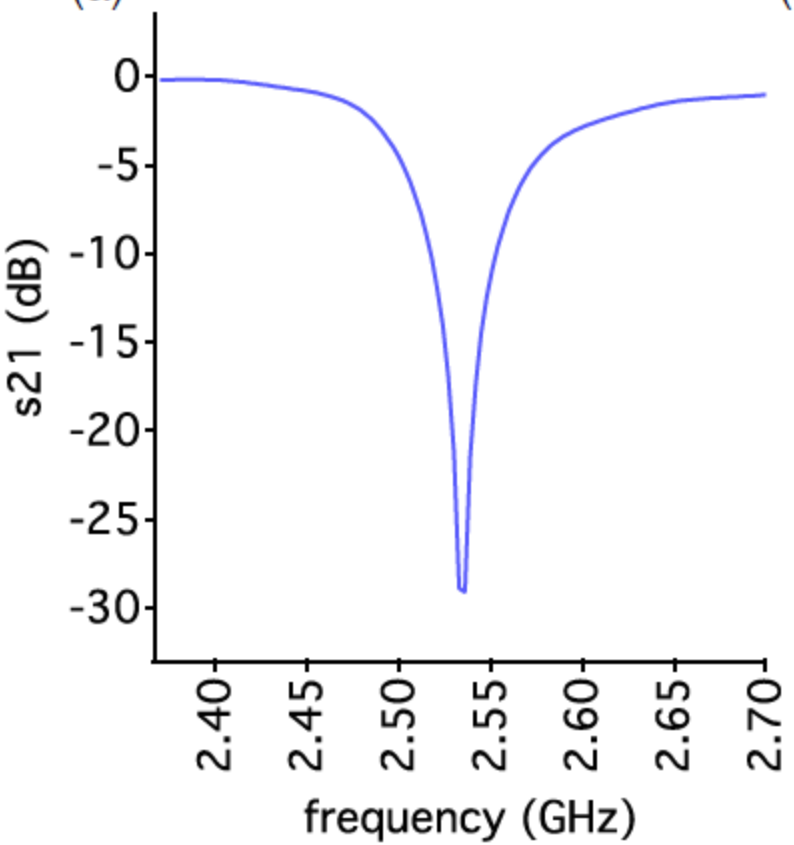
0
-5
-10
-15
-20
-25
-30
s21 (dB)
2.40
2.45
2.50
2.55
2.60
2.65
2.70
frequency (GHz)

(c)

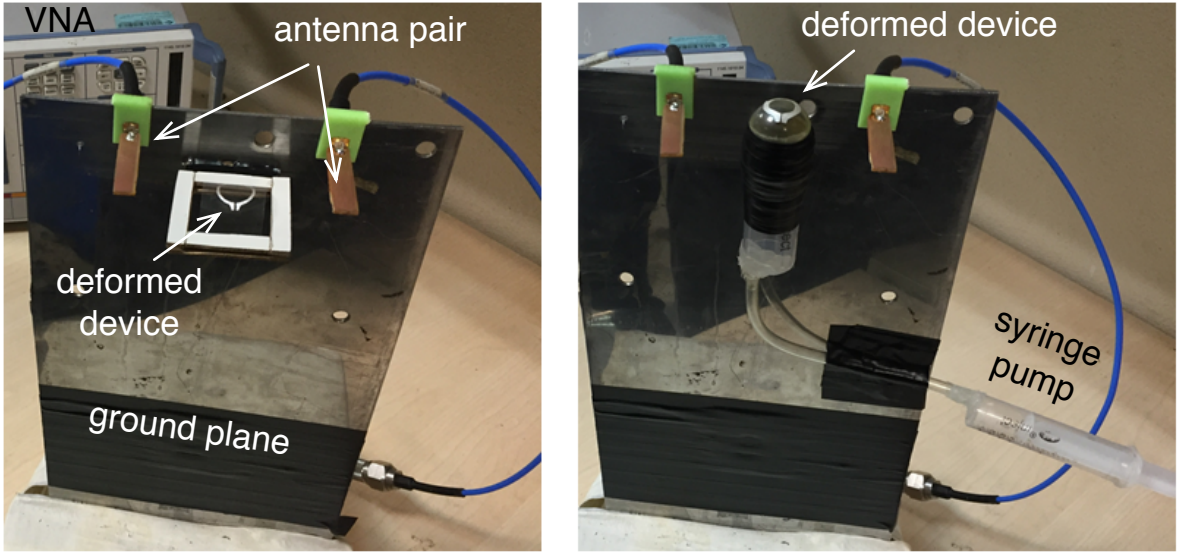
VNA
antenna pair
deformed
device
ground plane
deformed device
syringe
pump

(a) (b)

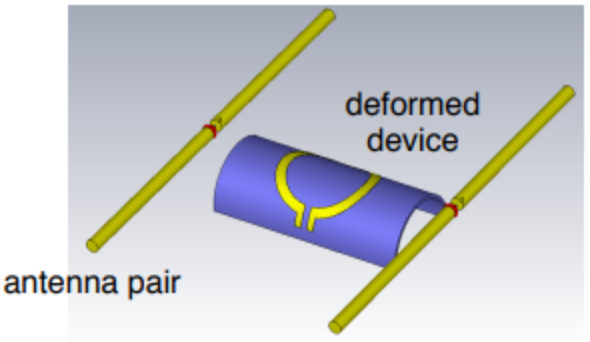
deformed
device
antenna pair

(a)

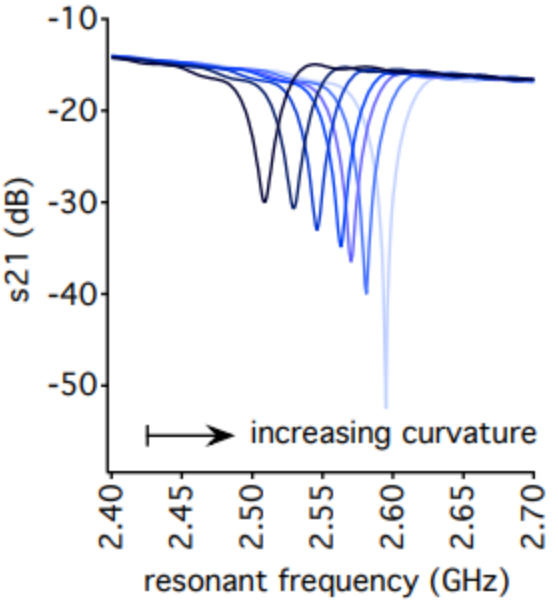
-10
-20
-30
-40
-50
s21 (dB)
increasing curvature
2.40
2.45
2.50
2.55
2.60
2.65
2.70
resonant frequency (GHz)

(b)

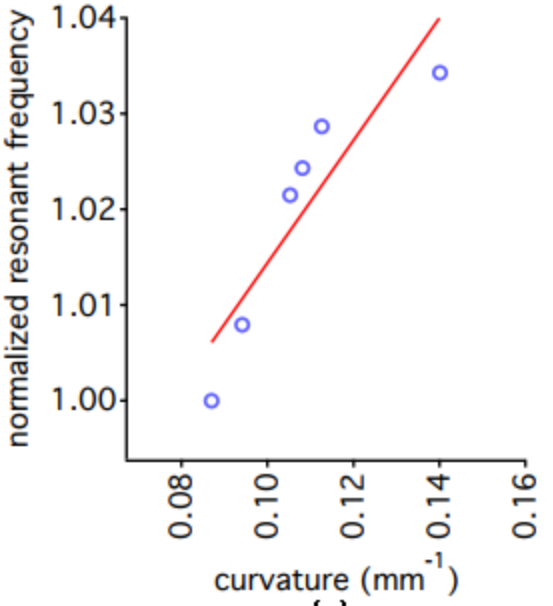
1.04
1.03
1.02
1.01
1.00
normalized resonant frequency
0.08
0.10
0.12
0.14
0.16
curvature (mm-1)

(c)

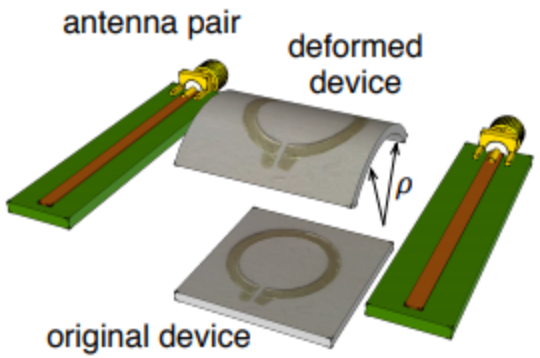
antenna pair
deformed
device
ρ
original device

(d)

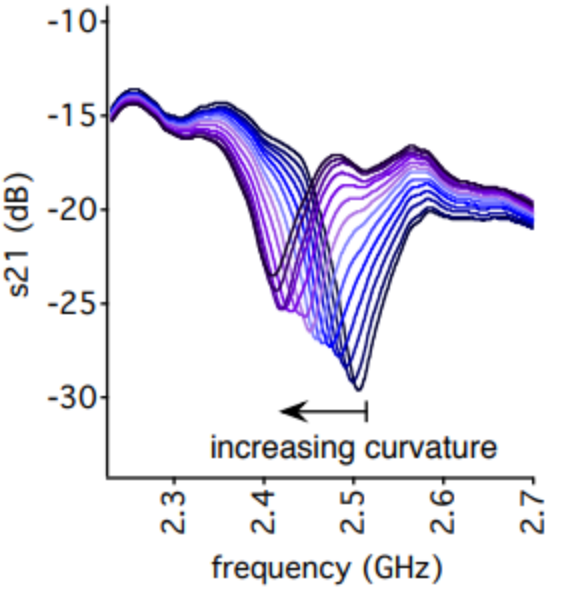
-10
-15
-20
-25
-30
s21 (dB)
increasing curvature
2.3
2.4
2.5
2.6
2.7
frequency (GHz)

(e)

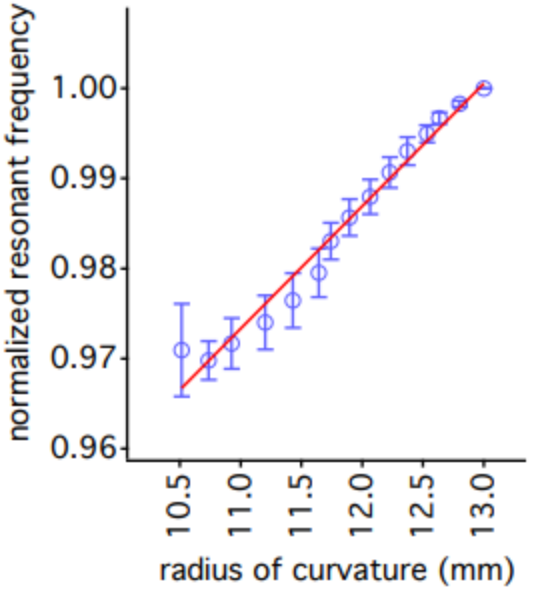
1.00
0.99
0.98
0.97
0.96
normalized resonant frequency
10.5
11.0
11.5
12.0
12.5
13.0
radius of curvature (mm)

(f)

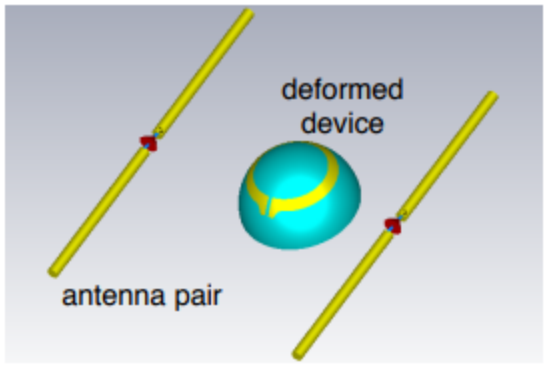
deformed
device
antenna pair

(a)

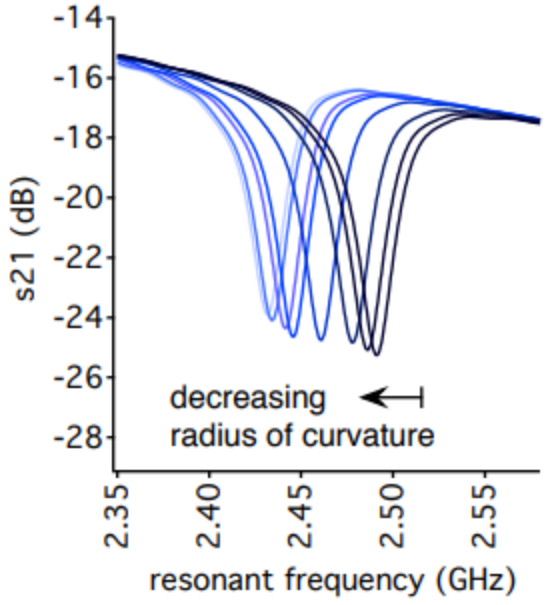
-14
-16
-18
-20
-22
-24
-26
-28
s21 (dB)
decreasing
radius of curvature
2.35
2.40
2.45
2.50
2.55
resonant frequency (GHz)

(b)

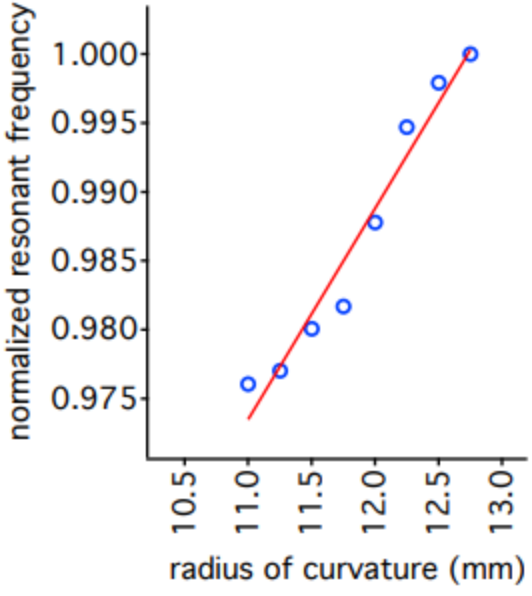
1.000
0.995
0.990
0.985
0.980
0.975
normalized resonant frequency
10.5
11.0
11.5
12.0
12.5
13.0
radius of curvature (mm)

(c)

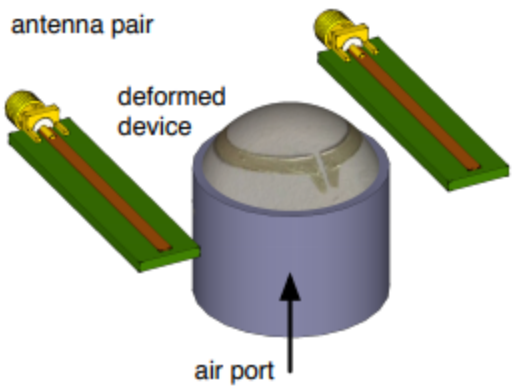
antenna pair
deformed
device
air port

(d)

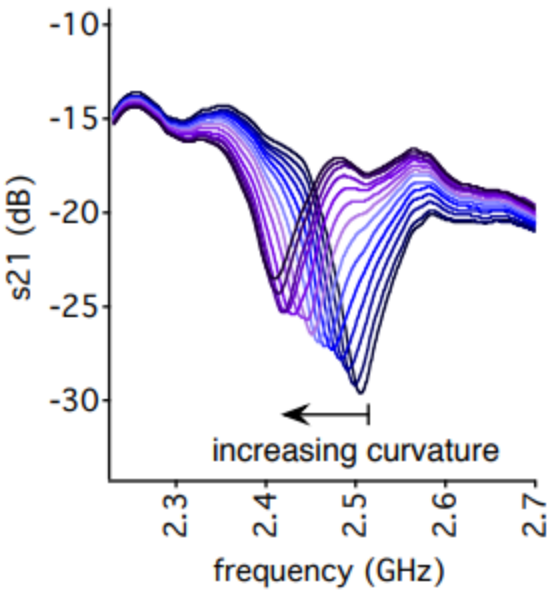
-10
-15
-20
-25
-30
s21 (dB)
increasing curvature
2.3
2.4
2.5
2.6
2.7
frequency (GHz)

(e)

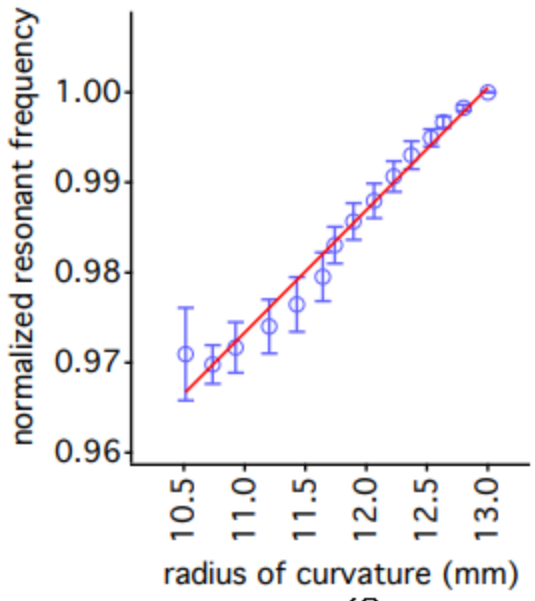
1.00
0.99
0.98
0.97
0.96
normalized resonant frequency
10.5
11.0
11.5
12.0
12.5
13.0
radius of curvature (mm)

(f)